Extraction of individual Pockels coefficients of thin films via interferometric reflection measurements

Journal of Physics: Photonics

PAPER

Extraction of individual Pockels coefficients of thin films via interferometric reflection measurements

Kobe De Geest[1,2], **Enes Lievens**[1,2], **Ewout Picavet**[1,3], **Klaartje De Buysser**[3], **Dries Van Thourhout**[2,4] and **Jeroen Beeckman**[1,*]

[1] Liquid Crystals & Photonics group, Department of Electronics and Information Systems, Ghent University, Technologiepark-Zwijnaarde 126, 9052 Ghent, Belgium
[2] Photonics Research Group, Department of Information Technology, Ghent University, Technologiepark-Zwijnaarde 126, 9052 Ghent, Belgium
[3] SCRiPTS group, Department of Chemistry,Krijgslaan 281 - building S3, 9000 Gent, Belgium
[4] IMEC, Technologiepark-Zwijnaarde 126, 9052 Ghent, Belgium
[*] Author to whom any correspondence should be addressed.

E-mail: jeroen.beeckman@ugent.be

Keywords: Pockels effect, ferroelectric thin films, $Pb(Zr,Ti)O_3$, $BaTiO_3$, electro-optic modulation

Supplementary material for this article is available online

OPEN ACCESS

RECEIVED
27 September 2024

REVISED
20 December 2024

ACCEPTED FOR PUBLICATION
10 January 2025

PUBLISHED
22 January 2025

Abstract

Ferroelectric thin films integrated on passive photonic platforms offer ways to achieve functionalities that are otherwise impossible or inefficient, such as electro-optic (EO) modulation, acousto-optic modulation or optical nonlinear conversion. Characterization methods of the EO properties of thin films are often only able to extract an effective EO response, while in many integrated photonic circuits it is one of the Pockels coefficients that determines the strength of the modulation. In this work, we demonstrate a new method to extract the r_{33} and the r_{13} coefficient independently by measuring the change in polarization and amplitude of light reflected at the sample, taking into account multiple reflections and interference effects. This method is verified for highly textured $Pb(Zr,Ti)O_3$ and $BaTiO_3$ thin films.

1. Introduction

Interest in ferroelectric thin films has grown during the past years because of their potential applications in photonic integrated circuits (PICs) [1–7]. Such materials often exhibit a large Pockels effect, which allows for fast, pure and low power optical phase modulation. Other methods such as thermal tuning are limited in speed and consume more energy. Carrier modulation in silicon photonics is widely used, but introduces small changes in absorption and leads to spurious amplitude modulations, which is unwanted for certain applications. By far the most mature and investigated material for electro-optic (EO) phase modulation is lithium niobate ($LiNbO_3$). Its relevant Pockels coefficient is well known from bulk crystal measurements and is around 30 pm V^{-1}. In the thin film lithium niobate technology the film is made from a bulk crystal and its EO coefficients are close to its bulk values [8, 9]. To further increase the use and functionalities of PICs, high speed EO modulators with a small footprint are desired, which requires an improvement in the phase modulation efficiency. The most straightforward way to achieve this is to use materials with large Pockels coefficients. Materials such as $Pb(Zr,Ti)O_3$ (PZT) and $BaTiO_3$ (BTO) are promising candidates, as they are known to have large Pockels coefficients as bulk materials. Several groups have been investigating these materials in the past years [10–15] to see if these values can also be obtained in their thin film counterparts. Several groups are also investigating different types of materials like silicon-organic hybrids [16–18], to achieve the same goal. In order to investigate these materials, accurate measurement methods for the Pockels coefficients in thin films are required.

Measurement techniques for bulk materials have been around for a long time and an overview of most of them can be found in [19]. However, applying these methods to thin films is not always straightforward as the signal typically scales with the propagation distance through the EO-layer, which is orders of magnitude

smaller in thin films than in bulk materials. Spectroscopic ellipsometry methods have been used to measure the Pockels coefficients accurately [20–22]. Here, a light beam impinges on the thin film obliquely and the polarization state of the reflected light is recorded to extract the EO response. The drawback of this method is that the thin film needs to be sandwiched between two electrodes that are large enough to accommodate for the beam size. The electric field is perpendicular to the substrate (i.e. and out-of-plane configuration), which is different from the in-plane field that is mostly used in integrated EO modulators with co-planar electrodes.

Another approach is given in [23], where the reflection at the material interface is modulated according to Fresnel equation of reflection. They claimed that this method can be applied to thin films as well. However this only holds true when there is only one reflection, i.e. for a non transparent thin film. This is often not the case for actual samples, which might even consist out of several transparent layers.

For thin film measurements the modulation of the light is very small when the beam passes through the layer perpendicularly since the propagation distance through the sample is limited to only a few hundred nanometer. One way to overcome this is to use a lock-in amplifier, which can detect very small signals as described in [24–26] where a setup is discussed to measure the effective Pockels coefficient ($r_{\text{eff}} = r_{33} - r_{13}$) of an epitaxially grown thin film of BTO. Their measurement setup is similar to a Sénarmont setup, having a polarizer and a half wave plate (HWP) before the sample and a quarter wave plate (QWP) and analyzer after the sample. The light power transmitted though the sample is modulated by applying a sinusoidal AC electric field and this small modulation amplitude can be measured using a lock-in amplifier. The power modulation comes from changes in the polarization state of the transmitted light due to the induced birefringence. In addition the angle of the analyzer is being swept in order to improve the accuracy allowing to measure a change of the polarization angle up to 10^{-5} degree. This type of setup has two major shortcomings. First, it requires a fully transparent sample at the wavelength of the measurement, including a non scattering backside. Second, it is only possible to measure the difference between r_{33} and r_{13} since it relies on a change in birefringence. The r_{eff} gives an indication of the magnitude of the EO effects, but is not the relevant parameter for integrated EO modulators where either the r_{33} or r_{13} is relevant depending on the waveguide geometry (TE or TM mode) and electrode design.

In this work we present a novel measurement method, which works in reflection and is able to measure both r_{33} and r_{13} independently in addition to r_{eff} allowing to determine their relative sign. The method takes into account the effect of multiple reflections at different material interfaces and interference effects resulting from these multiple reflections. This method, however, does not need special extra material layers such as done in the work of [27], but any material stack can be used. Because of those effects the modulation is not purely a result of retardation due to birefringence and thus no longer solely dependent on r_{eff}. To demonstrate the validity of this method, results are presented for thin films of fiber textured PZT and BTO deposited on silicon wafers with an intermediate silicon-oxide layer [14, 15].

2. Electro-optic modulation

The dielectric optical properties of a material are often expressed in terms of the dielectric permittivity tensor $\overline{\overline{\varepsilon}}$, which relates the dielectric displacement field $\overline{D}$ with the electric field $\overline{E}$. In the context of EO materials often the impermeability tensor is used $\overline{\overline{\eta}}$, which is the inverse of $\overline{\overline{\varepsilon}}$, such that $\overline{E} = \frac{1}{\varepsilon_0}\overline{\overline{\eta}} \cdot \overline{D}$. It is then assumed that the impermeability tensor can be expressed as a power series of the electric field [28]:

$$\eta_{ij} = \eta_{ij}^{(0)} + \sum_{k} r_{ijk} E_k + \sum_{kl} s_{ijkl} E_k E_l + \ldots \tag{1}$$

With r_{ijk} the Pockels coefficients and s_{ijkl} the Kerr coefficients. In this work we only look at the Pockels effect, which we can do since the Kerr effect is typically a few orders of magnitude smaller. In addition, any second or higher order effects are filtered out by the lock-in amplifier (see section 3.2). Due to symmetries in the crystal structure often a lot of tensor elements are zero. For bulk crystals, the EO coefficients are well known. Important materials are $LiNbO_3$ with $r_{13} = 9.6\,\text{pm}\,\text{V}^{-1}$, $r_{22} = 6.8\,\text{pm}\,\text{V}^{-1}$, $r_{33} = 30.9\,\text{pm}\,\text{V}^{-1}$ and $r_{42} = 32.6\,\text{pm}\,\text{V}^{-1}$ and BTO with $r_{13} = 8\,\text{pm}\,\text{V}^{-1}$, $r_{33} = 105\,\text{pm}\,\text{V}^{-1}$ and $r_{42} = 1300\,\text{pm}\,\text{V}^{-1}$ [29]. For thin films, the aim is to optimize the deposition process such that the values for the thin film approach the bulk values. For certain materials the values are close, but for other materials it is difficult to get thin film values that are as good as the bulk values [30].

Assuming a tetragonal crystal structure as it is the case for BTO [14, 31] and PZT near the morphotropic phase boundary [15, 32] and an applied electric field along the poling direction, electric field and c-axis of

the EO-material are both along the x direction and the impermeability tensor then becomes:

$$\overline{\overline{\eta}} = \begin{bmatrix} \eta_e^0 + r_{33}E & 0 & 0 \\ 0 & \eta_o^0 + r_{13}E & 0 \\ 0 & 0 & \eta_o^0 + r_{13}E \end{bmatrix}. \tag{2}$$

When probing the thin film with a light beam traveling along the z direction, the two linear polarization states of light encounter a different refractive index:

$$n_x \approx n_e - \frac{1}{2} n_e^3 r_{33} E \tag{3}$$

$$n_y \approx n_o - \frac{1}{2} n_o^3 r_{13} E. \tag{4}$$

The birefringence of the layer is then expressed as:

$$\Delta n = n_x - n_y \approx \Delta n(0) - \frac{1}{2}\left(n_e^3 r_{33} - n_o^3 r_{13}\right) E \approx -\frac{1}{2} n^3 r_{\text{eff}} E. \tag{5}$$

$\Delta n(0) = n_e - n_0$ is the birefringence of the material in the absence of an applied electric field. In the last step in equation (5) the approximation that $n_e \approx n_o \approx n$ is used.

For a more in-depth explanation of light propagation through anisotropic media and EO effects we refer the reader to [33].

2.1. Transmission

The effective Pockels coefficient can be measured by detecting the polarization change of a laser beam passing through the thin film [24]. Typically, linearly polarized light is impinging on the sample, polarized at a 45° angle with respect to the applied electric field and poling direction. A QWP then converts the light into elliptical polarization (almost circular assuming small retardation). Using another polarizer the changes in the retardation due to an applied electric field is then converted into a signal that is proportional to the applied electric field. A schematic of such a setup is shown in figure S1.

When a birefringent medium is inserted between crossed polarizers the transmission is given by $T = \sin^2(\Gamma/2)$ with Γ the retardation. In the case the retardation comes from the QWP and the sample, the transmission can be expressed as:

$$T = \sin^2\left(\pm\frac{\pi}{4} + \frac{\pi \Delta n d}{\lambda}\right) \tag{6}$$

$$= \frac{1}{2} \pm \frac{1}{2} \sin\frac{2\pi \Delta n d}{\lambda} \tag{7}$$

with d being the thickness of the thin film and λ the wavelength of light. In case the retardation is small the signal is indeed proportional to E:

$$T \approx \frac{1}{2} \mp \frac{\pi n^3 r_{\text{eff}} d}{2\lambda} E. \tag{8}$$

The $\pm$ in these equation is to include the possible 90° rotation of the QWP, which will be relevant for the discussion in section 2.2.2

2.2. Reflection

When using reflection of light to measure the EO effect, multiple reflections at several interfaces and their interference need to be considered. A simple reasoning can be made to show why this is the case for reflection, even though interference effects are typically ignored for transmission measurements. One can consider the simplest example of a single layer of EO-material in air with two material boundaries air-EO layer, as indicated in figure 1(a). The relative strength of the reflection at the first and second interface can be approximated with the Fresnel equations, equations (9) and (10)

$$R = \left(\frac{n_2 - n_1}{n_2 + n_1}\right)^2 \tag{9}$$

$$T = 1 - R. \tag{10}$$

Using $n_2 = 2$ for the EO-layer and $n_1 = 1$ for air, the two strongest reflections lead to a relative power of $R_0 = 0.11$ and $R_1 = 0.09$. Where R_0 is the reflected power at the first interface, equal to R and R_1 is the

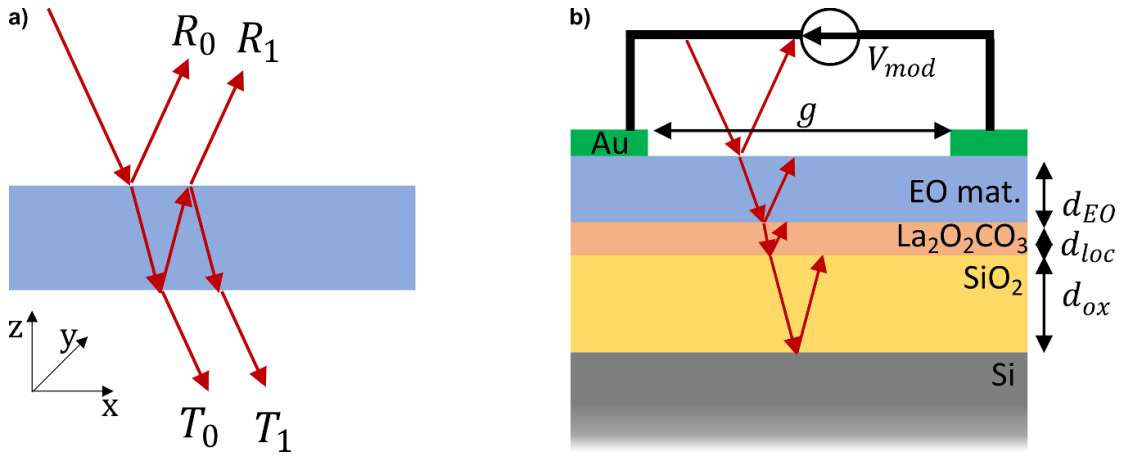

Figure 1. (a) Indication of multiple reflections in a single optical layer. (b) Schematic view of the different layers of the samples for measurements.

reflected power coming from reflection at the second interface, equal to $T \times R \times T$. These two reflection are relatively close in intensity and will interfere with each other. Changing the optical path near resonance can thus have a great effect on the reflected power. The same can be done for the transmitted light where the first two orders $T_0 = 0.79$ and $T_1 = 0.01$ are obtained with $T_0 = T \times T$ and $T_1 = T \times R \times R \times T$. T_0 is an order of magnitude larger than T_1. This indicates that interference effects play a much smaller role in transmission as compared to reflection.

The reasoning above is a strong oversimplification, but it shows why the reflection is not only modulated by a change in the retardation due to r_{eff} but also by changes in reflection coefficients at the material interfaces and changes in the interference of multiple reflections by a change of optical path length, $n\lambda$, in the EO layer. Due to these additional effects the reflected power is not a function of $r_{\text{eff}} = r_{33} - r_{13}$, but will instead depend on both r_{33} and r_{13}, so even if $r_{33} = r_{13} \neq 0$ a signal would be measured.

Due to these additional effects a simple adaptation of equation (8) is not possible. For this method an accurate calculation of the reflected light is needed.

2.2.1. Calculating reflection

Using a plane wave approximation, the reflection can be calculated for light polarized along n_e and n_o separately. Here, only perpendicular incidence of the light needs to be considered. This can be solved exactly by solving a set of linear equations linking the $\mathcal{E}$ and $\mathcal{H}$ field at all layer boundaries. We use rounded letters $\mathcal{E}$ and $\mathcal{H}$ to indicate that these are optical fields, in contrast to non rounded letter E, which denotes a (quasi-)static electric field. For this the Berreman method is used. The linear set of equations can be found in the supporting information (SI), (S1)–(S5). Figure 2 shows the measured reflection spectrum of the PZT sample alongside the simulated reflection spectrum obtained from these equations. It demonstrates that the model is correctly implemented.

2.2.2. Calculating change in reflection due to electric field

The setup used to measure the change in reflection is shown in figure 3. To control the polarization of the laser light a polarizer and HWP are used. The light is focused between interdigitated electrodes (IDT) on the sample using a strong lens. The reflected power is measured using a photodetector in front of which are a QWP and an analyzer used to convert change in polarization into a change in power. Since the change in power, due to an applied electric field, will be small an AC signal is applied to the device under test which allows us to use a lock-in amplifier to measure the small power modulation.

Several orientations of the optical components, HWP, QWP and polarizers, are possible. For ease of notation an overview of the different configurations used is given in table 1. Configuration 1 and 2 are the same as what is typically used for transmission measurements [24], where the light is polarized at 45° and a change in birefringence is measured. Since in reflection there is also a change in power configuration 3 and 4 will also result in a measurable signal even though the light will not experience any change in polarization, as it is polarized along one of the principle axis.

Light reflected at the sample can be calculated as a function of the applied electric field using equations (3) and (4) for the refractive indices. The effect of the QWP and analyzer can be accounted for using the Jones Matrix formalism. From this, the power on the detector can be calculated as a function of the

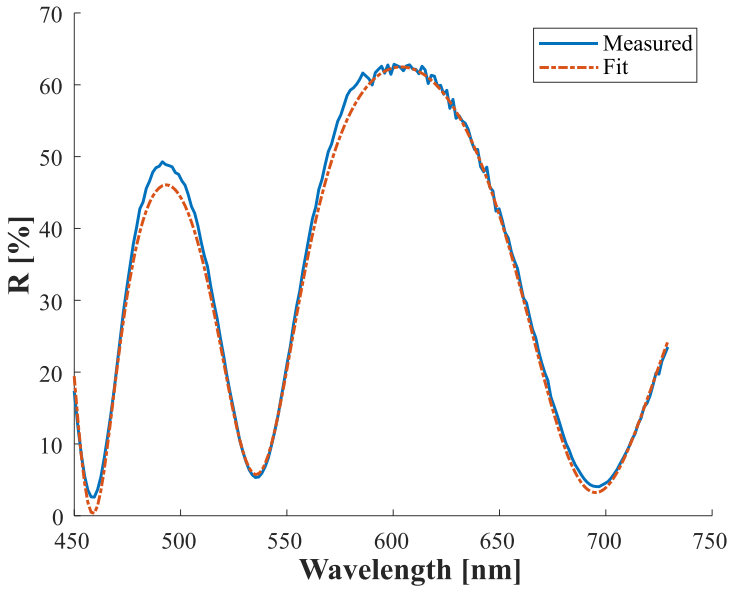

Figure 2. Measured and simulated reflection spectrum of the PZT sample. The good overlap between measurement and simulation demonstrates that the equations to calculate the reflection are correctly implemented.

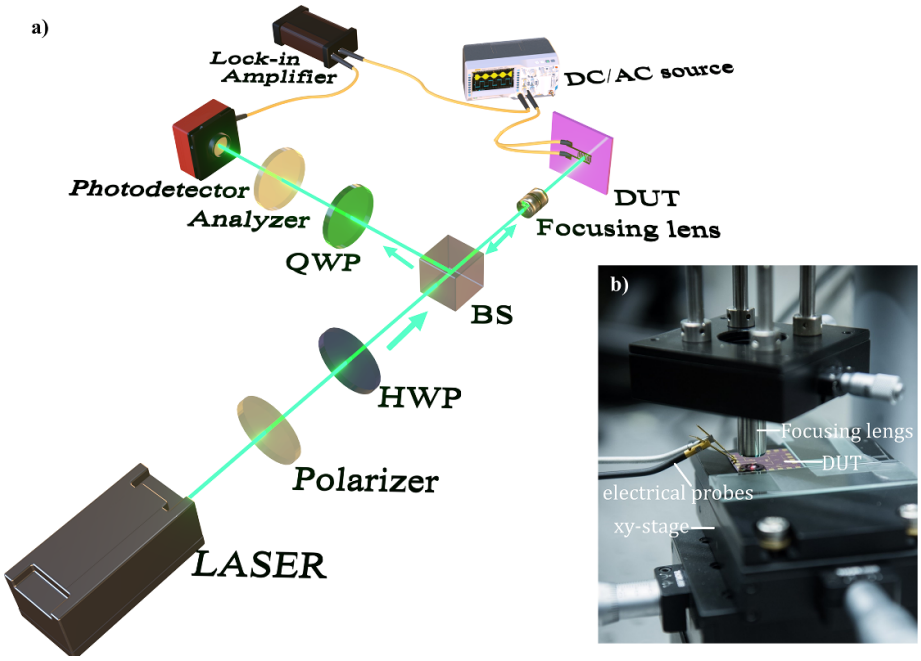

Figure 3. (a) Schematic of the measurement setup used to measure the Pockels effect in reflection. Incoming laser light passes through a polarizer and a half-waveplate (HWP) to control the incident polarization, a focusing lens is used to focus the light between the IDT. The reflected light is redirected using a beamsplitter (BS) after which it passes through a quarter-waveplate (QWP) and analyzer to convert the change in polarization into amplitude modulation. (b) Picture of sample in the setup.

Table 1. Naming of the different configurations of the optical components used within this work.

Name	E-field	Incoming polarization	QWP	Analyzer
Configuration 1	0°	45°	0°	135°
Configuration 2	0°	45°	90°	135°
Configuration 3	0°	90°	–	–
Configuration 4	0°	0°	–	–

Table 2. Parameter values used in example calculations.

Symbol	Value	Description
d_{EO}	0–300 nm	Thickness of the EO-layer
d_{ox}	480 nm	Thickness of the SiO_2-layer
d_{loc}	15 nm	Thickness of the intermediate layer
λ	515 nm	Wavelength used
E	1 V μm^{-1}	Amplitude of modulation electric field
n_{EO}	2.4	Refractive index EO-layer
n_{loc}	1.75	Refractive index seed layer
r_{13}	10 pm V^{-1}	Pockels coefficient
r_{33}	100 pm V^{-1}	Pockels coefficient

applied electric field. However, the lock-in amplifier used in the measurement setup measures the amplitude of the detected sine-wave. We are thus interested in: $(R(-E) - R(E))/2$, which is the amplitude when a small AC electric field, with amplitude equal to E, is used to modulate the signal. This can then also be normalized by dividing by the unmodulated reflected power, which is given by $R(0)$. For small values of E, this response is still a linear function of the amplitude of the applied AC electric field and it is the slope of this function, which is related to the Pockels coefficients. This slope can be found by dividing $(R(-E) - R(E))/(2R(0))$ by the amplitude E, which in the simulations is typically taken to be 1 V μm^{-1} and in the measurements assumed to be $E = V_{mod}/g$ with g the distance between the electrodes. This results in equation (11), which is a function of the sample parameters (i.e. layer thickness, refractive index,...) and the Pockels coefficients r_{13} and r_{33}. Equation (12) gives this same signal but expressed in parameters from the measurement setup (see section 3.2), where V_{PD_0} is the photodetector voltage without AC electric field ($E = 0$V), $\frac{\partial V_{VD}}{\partial V_{mod}}$ is the change in photodetector voltage due to the AC applied electric field and g is the spacing between the electrodes. From these equations (equations (11) and (12)), the Pockels coefficients can be calculated if all other parameters are known. Note that these parameters are contained in the function R, which depends on the thickness and refractive index of all the layers of the sample. To determine the unknown parameters, d_{ox}, d_{EO} and n_{EO} the reflection spectrum of the sample is measured and the same simulation code is used to fit these parameters, see figures S3 and S4 in SI

$$S = \frac{R(-E) - R(E)}{2R(0)} \frac{1}{E} \tag{11}$$

$$S = \frac{g}{V_{PD_0}} \frac{\partial V_{PD}}{\partial V_{mod}}. \tag{12}$$

2.2.3. Example simulations

The resonance behaviour is illustrated in figure 4, where a sweep over the layer thickness is carried out for various configurations. The parameters used are shown in table 2. Figure 4(a) shows the signal S as well as the reflected power without electric field for the simple case of air/ EO-layer/ air as a function of the thickness of the EO-layer. It is clear that there is a strong resonance, due to the normalization, close to the point of destructive interference and zero light reflection. However even if the signal is not normalized, by the reflected power, the relation with respect to the thickness remains non-linear, as shown in figure 4(b) where the same signal is shown but without the normalization. Thus a full calculation of the reflection is needed in order to analyze a signal obtained in reflection.

In practice, the devices under test do not consist of a single layer. In this work the samples consist of a thin film of PZT or BTO on top of a stack of $Si/Si_2O_3/La_2O_2CO_3$ as outlined in table 2 [13–15] (see figure 1(b) and section 3.1). Figure 4(c) shows simulation results for such a configuration. The relation between the signal strength and the thickness of the EO-layer for two orientations of the QWP is shown, as well as the linear graph expected by the classic model used for transmission. The graph for the classic model is given by the following equation:

$$S_{\text{Classic model}} = \frac{(r_{33} - r_{13})\, n_{EO}^3 \pi\, 2d}{\lambda} \tag{13}$$

which comes from equation (8) with the exception that d is replaced by $2d$. The signal with the QWP at 0° is multiplied by −1 for easier comparison. A zoomed in region is shown in the inset, which shows that between the resonances the signal is also within the measuring range. It is clear from the graphs that the simple transmission model is not acceptable for the reflection setup. In case the measured power modulation would

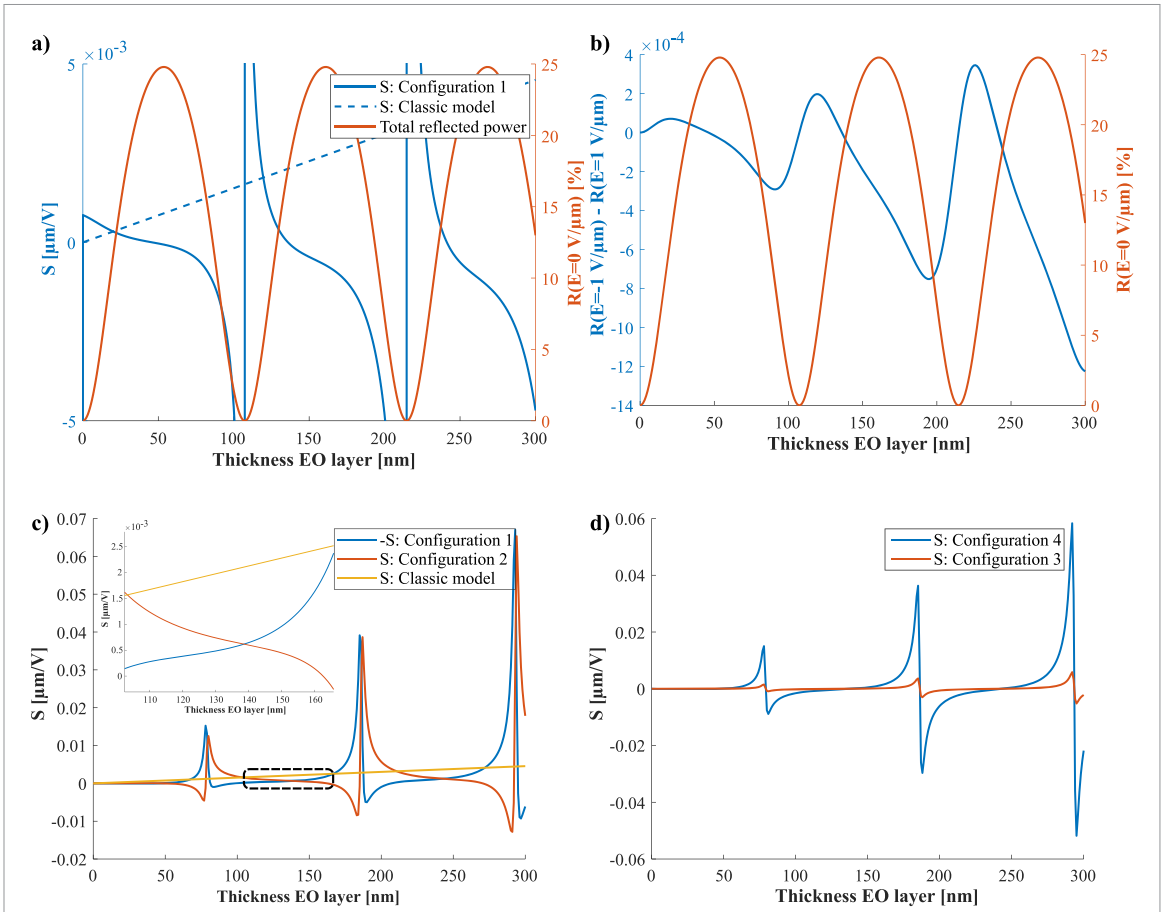

Figure 4. Various simulations sweeping over the thickness of the EO layer, showing the non-linear relation between signal and thickness caused by interference between multiple reflections. (a) Shows the signal S as well as the reflected power for a single layer stack, the EO layer. Incoming polarization @ 45° with respect to applied electric field, QWP @ 0°. (b) Shows the same but only the numerator of the signal S (i.e. the not normalized signal). (c) and (d) show the signal S for a more realistic material stack, see table 2, for various configurations of incoming polarization and QWP orientations, see table 1. Inset in (c) shows zoomed in region.

only be caused by the birefringence, then rotating the QWP would only change the sign of the signal, see equation (8). The fact that rotating the QWP by 90° does not simply result in a change of sign comes from the additional power modulation caused by the change in reflected power.

Thus measuring with the QWP once at 0° and once at 90°, configuration 1 and 2, two different signals will be recorded, $S_1(r_{13}, r_{33})$ and $S_2(r_{13}, r_{33})$, which both depend on both r_{13} and r_{33}, which we want to extract. The way it is solved, in this work, is by subtracting the average of both signals from one of the signals, $S' = S_1 - (S_1 + S_2)/2$. This 'corrected' signal $S'(r_{\text{eff}})$ only depends on r_{eff} (see SI for proof), which can then be obtained from the simulations. Once r_{eff} is known, we can calculate r_{13} and r_{33} from the original signals $S_1(r_{33} - r_{\text{eff}}, r_{33})$, $S_1(r_{13}, r_{13} + r_{\text{eff}})$ and/ or $S_2(r_{33} - r_{\text{eff}}, r_{33})$, $S_2(r_{13}, r_{13} + r_{\text{eff}})$.

Up to now, the arrangement of optical components, HWP, QWP and polarizers, was kept the same as used in a typical transmission measurement, configuration 1 and 2. However, since in reflection there is a power modulation from the change in refractive index, this is not required. A more simple arrangement can be considered, configuration 3 and 4 where the incoming light is polarized either parallel to the polarization and electric field or perpendicular to it. Incoming light will not experience any change in polarization after passing trough the sample, thus the QWP and analyzer after the sample are left out. This makes the signal dependent only on either r_{33} or r_{13} respectively. The expected signal, as a function of the thickness, is shown in figure 4(d). Even without phase retardation, the signal can be large enough to be measured.

Note that in all these examples, the signal can be both positive or negative. This can be understood from equation (11) where the numerator can be either positive or negative. The way this is detected, in the actual setup, is by looking at the phase measured by the lock-in amplifier. This gives the phase difference between the applied electric signal and the measured signal. On its own this phase does not tell anything but if a shift of 180° is detected we know the signal changed sign. In the transmission setup a change in sign can be achieved by changing the poling direction of the sample, rotating the QWP 90° from 0° to 90° or equivalently changing the polarization of the incoming light from +45° to −45° using the HWP. In

reflection, changing the poling direction will also change the sign of the signal, as this is equivalent with changing E with $-E$. However, the response for configuration 1 and 2 in reflection also differ in amplitude not just in their sign, see figure 4(c). The reason why it is important to note that a change in sign can be observed, is because in the reflection setup this will allow to determine the relative sign of r_{13} and r_{33} i.e. determine whether they have the same sign or different sign.

2.2.4. Limitations and accuracy

Just like most measurement techniques, the one presented in this work also comes with some shortcomings and limitations. The main difficulty lies in the fact that the accuracy can be heavily influenced by errors in the fitted layer thicknesses and refractive indices of the different materials, present in the stack. In a transmission measurement where the response scales with a power of 3 of the refractive index and linear with the layer thickness of only the EO layer. This means that slight variations on the refractive index can lead to large variations in the extracted EO coefficient. In the reflection setup, the response is depending on the properties of all the layers. Fortunately, the different layer thicknesses can be somewhat freely chosen (e.g. the silicon dioxide layer thickness) and thus be tuned away from these resonant regions, such that the measurements can be performed with high tolerance on these parameters. In this work, we only use the reflection spectrum, but additional techniques may be used to determine the layer parameters more accurately such as ellipsometry, optical profilometry or FIB-SEM. In addition one could do the reflection measurement with different laser wavelengths, instead of a single wavelength measurement, to improve accuracy.

3. Experimental verification of the model

3.1. Sample preparation

The samples are prepared by depositing PZT(52/48) or BTO onto a double sided polished silicon wafer with 500 nm oxide according to the process described in [14, 15]. This yields for both a fiber textured a-axis oriented thin film. A Ti/Au metal IDT pattern is then deposited using a combination of conventional UV lithography, e-gun evaporation and lift-off. One of the samples can bee seen in figure 3(b).

3.2. Setup

The setup uses a green laser diode, Roithner dot laser CW520-05, with a wavelength of 515 nm. The laser beam is focused between two electrodes separated 10 μm apart. A Thorlabs PDA100A2 photodetector is used in combination with the Anfatec USB Lock-In amplifier, including a summing 100x amplifier to deliver the desired voltage signal to the sample, namely a high DC voltage modulated with a $5V_{\text{rms}}$– 25 kHz AC sine wave. During a measurement the laser scans over the sample, see figure S6 , the signal will be largest when the light is focused in the middle between two electrodes. This way it is assured that each measurement measures in the middle between the electrodes and that there is no shift between different measurements.

3.3. Measurements

To verify the model, the Pockels coefficients of two different EO thin films, BTO and PZT, are determined in two different ways using the reflection setup. The first method uses the same configuration of the optical components as the conventional transmission measurements and the QWP is rotated 90° to get the two signals needed to calculate r_{13} and r_{33}, configuration 1 and 2. The second method has the linear polarization of the incoming light orthogonal or parallel to the electric field to measure r_{33} and r_{13} independent of each other, configuration 3 and 4. In addition to the AC field a DC bias voltage is used to align the crystals c-axis parallel to the electric field. An electric field of 5 V μm^{-1} is used for this, which is sufficiently large to be in the saturation regime for both samples resulting in near maximum response.

3.4. Results and discussion

Figure 5 shows the data that is measured on the BTO sample, while a positive DC bias of 5 V μm^{-1} is applied. The total reflected power is shown in figure 5(a) as the voltage measured by the photodetector. The power varies as function of the position showing the reflection on the electrodes (maximum reflection) and between the electrodes (minimum reflection). Figure 5(b) shows the amplitude detected by the lock-in amplifier and as expected when the laser is focused on the electrodes no signal is detected. Also the phase difference between the applied AC field and the measured signal is shown in figure 5(c), this is used to determine the relative sign between measurements.

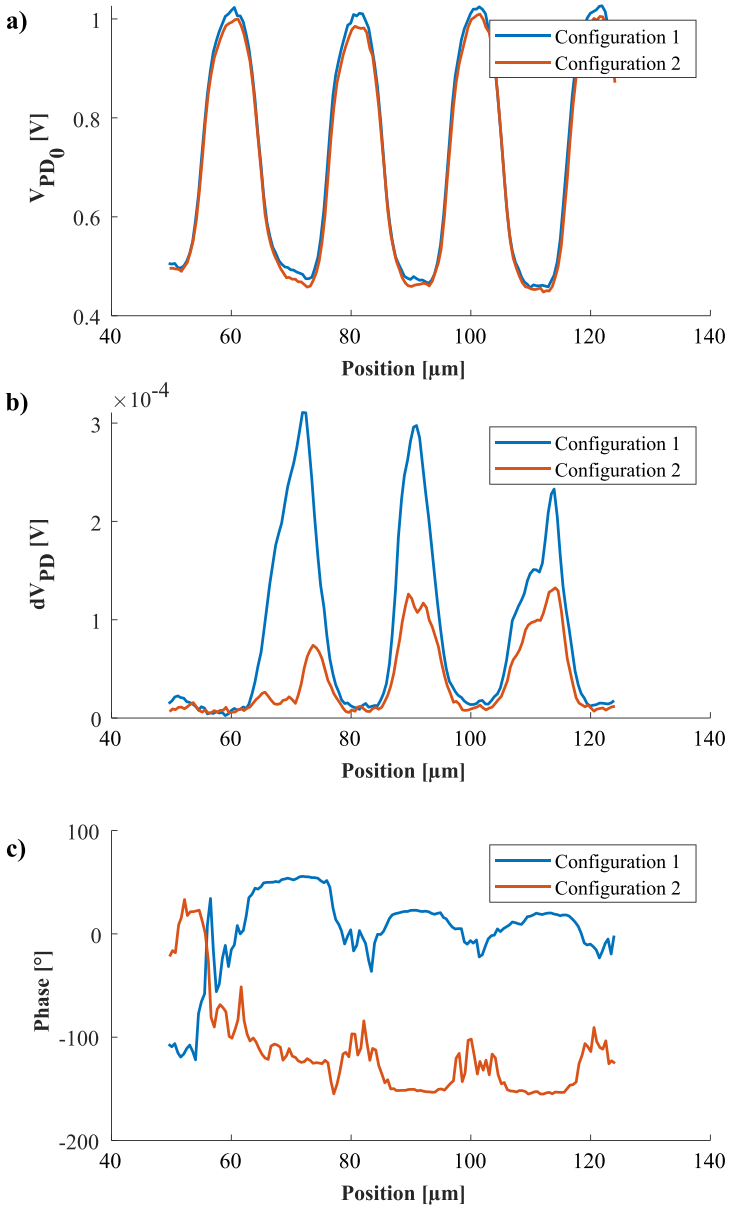

Figure 5. Data measured on BTO sample with 5 V μm^{-1} DC bias, (a) total voltage of photodiode, (b) amplitude measured by the lock-in amplifier, (c) phase measured by the lock-in amplifier.

This data is then converted to the normalized signal S, from which the Pockels coefficients are calculated. In figures 6 and 7 the analysed data of the different measurements are shown. First thing to note is the good match between the results for both methods described earlier. This is a good indication that the provided theory is correct and sufficient to describe the reflection setup since both methods are analyzed independent of one another. Additionally, a large signal is obtained even without any phase retardation effects, unlike what is the case in the similar transmission setup, further showing that the provided theory is correct and that this change in reflection coefficient can not be neglected. This gives a new and simple way to measure and characterize the more relevant r_{13} and r_{33} coefficients compared to the typically measured r_{eff} obtained from transmission setups.

Additionally, it is possible to derive the relative sign between r_{13} and r_{33}. In this case it is found for both the BTO sample as the PZT sample that $r_{13}r_{33} < 0$. This is directly evident from the change in sign between the measurements in configuration 3 and 4. As for those measurements the only factor, based on

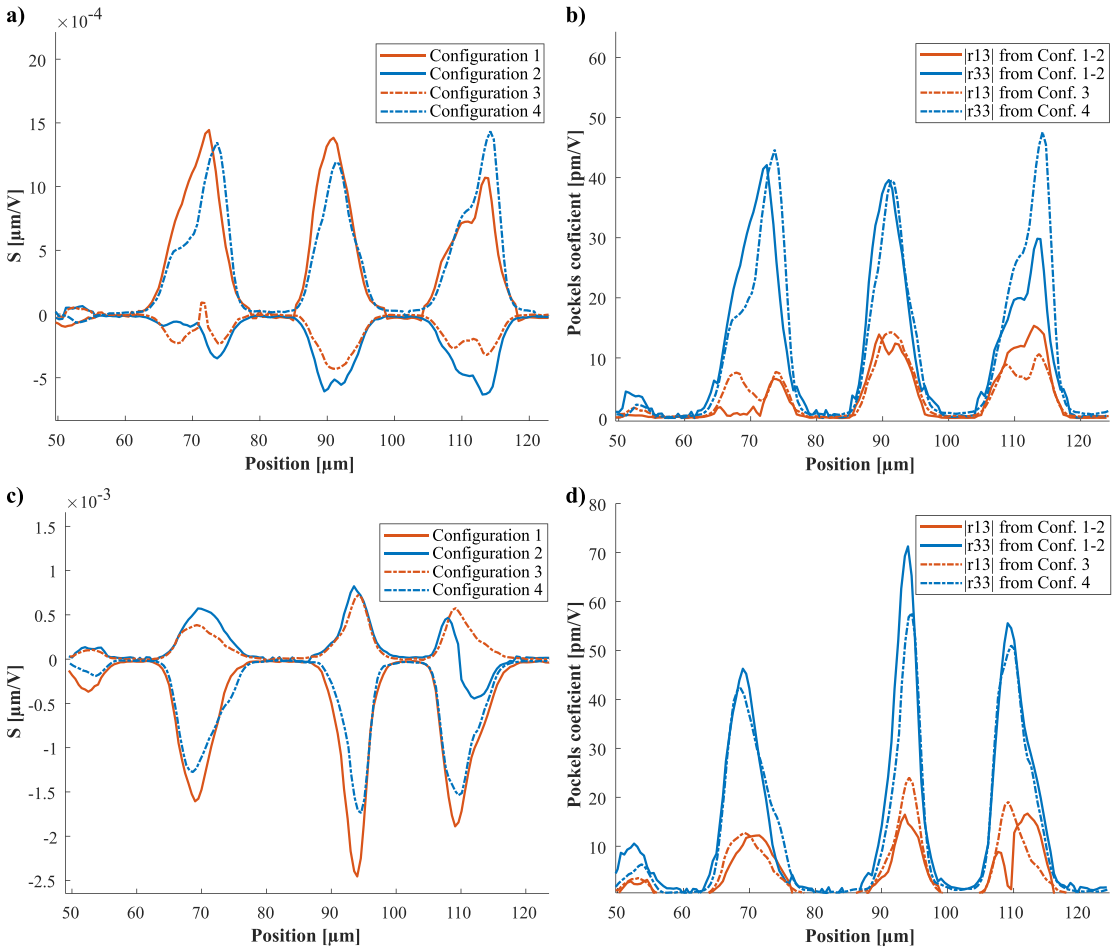

Figure 6. Measured (a), (c) and analyzed (b), (d) results for a BTO thin film. (a) and (b) Result with a positive DC bias of 5 V μm^{-1} to pole the domains. (c),(d) Result with a negative DC bias of 5 V μm^{-1} to pole the domains.

equations (3), (4) and (11), that can change in sign is the Pockels coefficient. Note that in figure 6(b),(d) and 7(b),(d) the absolute value of r_{13} and r_{33} is shown for easier comparison. We believe that this negative sign originates from the poly-crystalline structure of the samples. The explanation for this is out of the scope for this article and is planned for future work.

For BTO the obtained values are around 70 pm V^{-1} for r_{33} and around 20 pm V^{-1} for r_{13}. The effect is also the strongest in the middle between the two electrodes. For one of the measurements in figure 6 the signal gradually decreases and changes sign which could be caused by a small region in the sample that did not change its polarization and is still aligned opposite to the electric field.

For PZT values around 30 and 5 pm V^{-1} are obtained. For the r_{33} the signal is enhanced close to the edge of the electrodes. This can have several reasons. One of which is the electric field having a small vertical component at the edge of the electrodes. This would cause the r_{51} Pockels coefficient to have an effect as well. The reason we do not see this for the BTO sample could be due to its larger dielectric constant making the field more homogeneous or be due to the fact that the PZT actually consists of both a tetragonal phase and a rhombohedric phase unlike the BTO, which consist only out a tetragonal phase [14, 15]. This enhanced effect close to the electrodes might be utilized inside waveguide structures by clever design of the electrodes like the work done in [34], where 3D poling is used to obtain stronger Pockels response.

3.5. Comparison against established measurement method

To show that the obtained values are correct, a third sample was measured both in the reflection setup presented in this work as well as in the already established transmission setup [24]. The sample consists of a BTO thin film, with alternate recipe, on the same SiO_2/Si substrate. The results are shown in figure 8, both setups give a r_{eff} of 120–125 pm V^{-1}. These results further show that r_{eff} is not a good figure of merit as it can

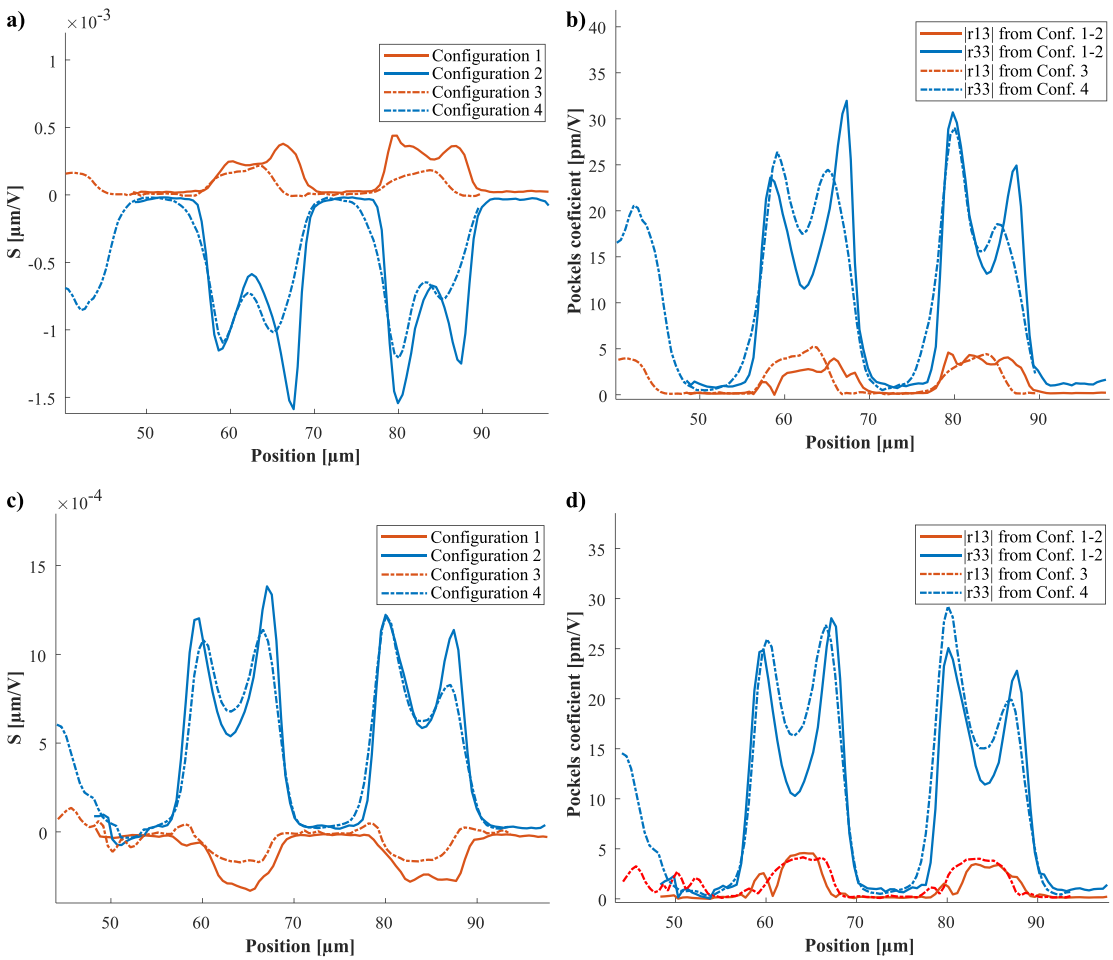

Figure 7. Measured (a), (c) and analyzed (b), (d) results for a PZT thin film. (a) and (b) Result with a positive DC bias of 5 V μm^{-1} to pole the domains. (c),(d) Result with a negative DC bias of 5 V μm^{-1} to pole the domains.

be seen that in this sample r_{13} and r_{33} are approximately equal in magnitude. Since for the targeted application of an integrated phase modulator, it will be the r_{33} coefficient that will be critical for TE guided modes, choosing the material with larges r_{eff} will not necessarily give the best performance. This can be seen by comparing with the results shown in figure 6 where a much smaller r_{eff} of 90 pm V^{-1} is found even though the r_{33} is approximately the same.

4. Conclusion

This work discusses and demonstrates, a new way of measuring Pockels coefficients in thin films. Unlike previous methods it is able to determine both r_{13} and r_{33} independent of each other. This new method allows for a bigger range of wavelengths and substrates to be used since it does not rely on transmission through the sample. The measurement results given in section 3.4 confirm the theoretical discussion given in section 2.2. From the results it is obtained that for our poly-crystalline fiber textured thin film PZT and BTO $r_{13_{\text{avg}}} r_{33_{\text{avg}}} < 0$, which we belief to be resulting from their random in-plane orientation and will be further investigated in future work. This extra insight is also important for waveguide structures as the random in-plane orientation will also lead to r_{51} contributions for TE polarized light. Furthermore by sweeping the laser over the IDT electrodes a clear picture of the non-uniformity of the Pockels effect between the electrodes is obtained.

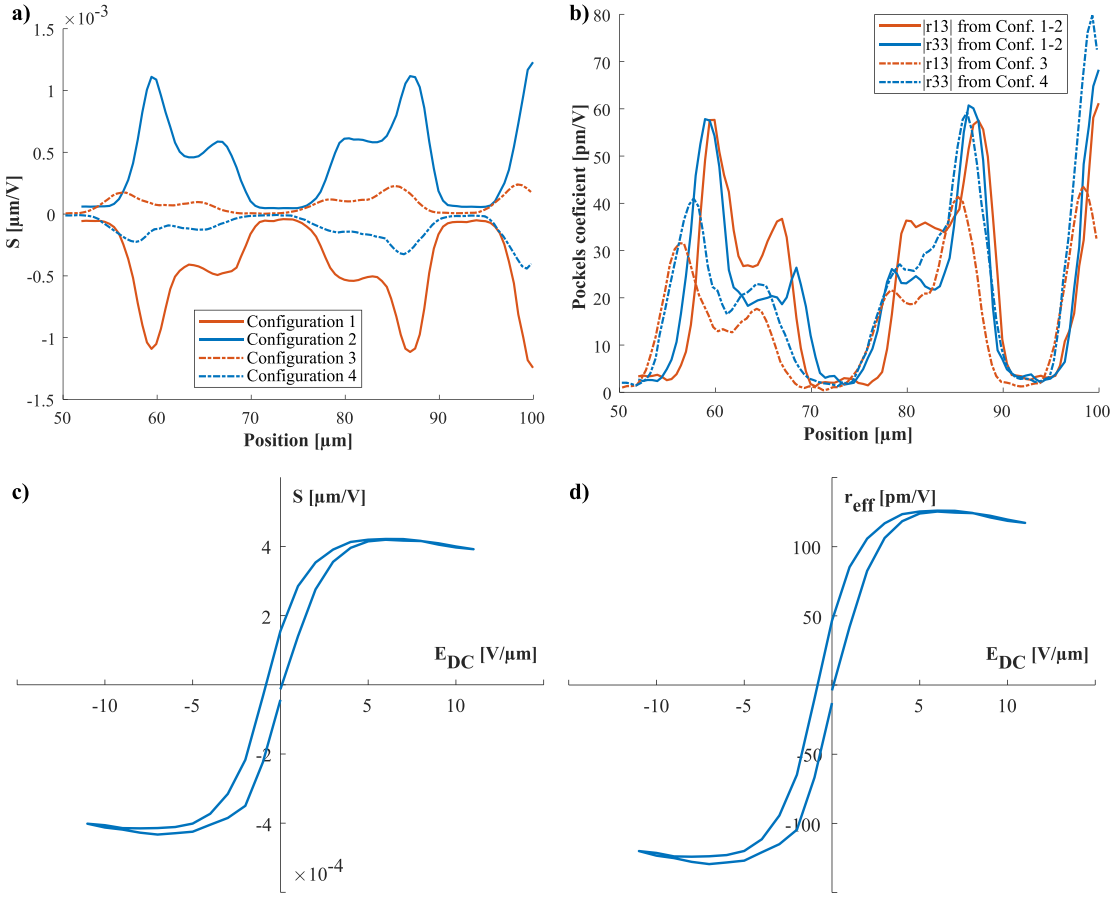

Figure 8. Electro optic measurements on thin film BTO. (a) and (b) Reflection measurements with positive DC bias of 5 V μm^{-1}. (c) (d) Transmission measurement of r_{eff} as function of applied DC-field. (a) and (c) show the normalized signal (b) and (d) the calculated Pockels coefficients..

Data availability statement

All data that support the findings of this study are included within the article (and any supplementary files).

Acknowledgment

This work was financially supported by Horizon Europe Project VISSION (Grant ID: 101070622).

ORCID iDs

Kobe De Geest https://orcid.org/0000-0002-5669-975X
Enes Lievens https://orcid.org/0009-0001-9867-4665
Ewout Picavet https://orcid.org/0000-0001-8196-2807
Klaartje De Buysser https://orcid.org/0000-0001-7462-2484
Dries Van Thourhout https://orcid.org/0000-0003-0111-431X
Jeroen Beeckman https://orcid.org/0000-0002-0711-2465

References

[1] Abel S *et al* 2018 *Nat. Mater.* **18** 42–47
[2] Sinatkas G, Christopoulos T, Tsilipakos O and Kriezis E E 2021 *J. Appl. Phys.* **130** 010901
[3] Xu M *et al* 2020 *Nat. Commun.* **11** 6160
[4] Xiong C, Pernice W H P and Tang H X 2012 *Nano Lett.* **12** 3562–8
[5] Wen Y *et al* 2024 *Adv. Opt. Mater.* **12** 88
[6] Zhang L *et al* 2024 *Adv. Photon. Nexus* **3** 066005
[7] Zhou W *et al* 2024 *Opt. Lett.* **49** 6353–6
[8] Sulser F, Poberaj G, Koechlin M and Günter P 2009 *Opt. Express* **17** 20291–300
[9] Rabiei P and Gunter P 2004 *Appl. Phys. Lett.* **85** 4603–5

[10] Alexander K, George J P, Verbist J, Neyts K, Kuyken B, Van Thourhout D and Beeckman J 2018 *Nat. Commun.* **9** 3444
[11] Ban D, Liu G, Yu H, Wu Y and Qiu F 2022 *J. Lightwave Technol.* **40** 2939–43
[12] Eltes F *et al* 2020 *Nat. Mater.* **19** 1164–8
[13] Picavet E, Rijckaert H, Solano E, Bikondoa O, Gutierrez Fernandez E, Paturi P, Van Bossele L, Vrielinck H, Beeckman J and De Buysser K 2023 *J. Mater. Chem.* **11** 7705–13
[14] Picavet E *et al* 2024 *Adv. Funct. Mater.* **34** 2403024
[15] Picavet E *et al* 2024 *ACS Appl. Mater. Interfaces* **16** 41134–44
[16] Kieninger C *et al* 2020 *Opt. Express* **28** 24693–707
[17] Wolf S *et al* 2018 *Sci. Rep.* **8** 2598
[18] Steglich P *et al* 2021 *J. Phys. Photon.* **3** 022009
[19] Aillerie M, Théofanous N and Fontana M 2000 *Appl. Phys.* B **70** 317–34
[20] Akazawa H and Shimada M 2005 *J. Appl. Phys.* **98** 113501
[21] Kang T D, Xiao B, Avrutin V, Özgür U, Morkoc H, Park J W, Lee H S, Lee H, Wang X and Smith D J 2008 *J. Appl. Phys.* **104** 093103
[22] George J P, Smet P F, Botterman J, Bliznuk V, Woestenborghs W, Van Thourhout D, Neyts K and Beeckman J 2015 *ACS Appl. Mater. Interfaces* **7** 13350–9
[23] Kniazkov A V 2016 *Tech. Phys.* **61** 631–4
[24] Abel S, Caimi D, Sousa M, Stöferle T, Rossel C, Marchiori C, Chelnokov A and Fompeyrine J 2012 Electro-optical properties of barium titanate films epitaxially grown on silicon fintro_Oxide-based Materials and Devices III *J Int. Society for Optics and Photonics* (Spie) vol 8263, ed F H Teherani, D C Look and D Rogers p 82630Y
[25] Abel S *et al* 2013 *Nat. Commun.* **4** 1671
[26] Kormondy K J *et al* 2017 *Nanotechnology* **28** 075706
[27] Villringer C, Steglich P, Pulwer S, Schrader S and Laufer J 2021 *Opt. Mater. Express* **11** 3801–11
[28] Boyd R 2008 *Nonlinear Optics* 3rd edn (Academic)
[29] Wen Y, Chen H, Wu Z, Li W and Zhang Y 2024 *APL Mater.* **12** 020601
[30] Abel S and Fompeyrine J 2016 *Electro-Optically Active Oxides on Silicon for Photonics* vol 8 (World Scientific) pp 455–501
[31] Buscaglia V, Buscaglia M T and Canu G 2021 $BaTiO_3$-based ceramics: fundamentals, properties and applications *Encyclopedia of Materials: Technical Ceramics and Glasses M* Pomeroy (Elsevier) pp 311–44
[32] Noheda B, Gonzalo J A, Cross L E, Guo R, Park S-E, Cox D E and Shirane G 2000 *Phys. Rev.* B **61** 8687–95
[33] Steglich P and Kehrein A 2024 *J. Opt. Soc. Am.* B **41** 2191–210
[34] Suraj S and Selvaraja S K 2023 *3d Poling and Drive Mechanism for High-Speed pzt-on-soi Electro-Optic Modulator* (*Cleo 2023*) (Optica Publishing Group) p JW2A.128